Journal of Sol-Gel Science and Technology (2019) 92:496–505
https://doi.org/10.1007/s10971-019-05034-y

ORIGINAL PAPER: NANO- AND MACROPOROUS MATERIALS (AEROGELS, XEROGELS, CRYOGELS, ETC.)

Check for updates

# The influence of CTAB/Si ratio on the textural properties of MCM-41 prepared from sodium silicate

E. V. Vyshegorodtseva[1] · Yu.V. Larichev[2,3] · G. V. Mamontov[1]

Received: 20 December 2018 / Accepted: 21 May 2019 / Published online: 1 June 2019


## Abstract

The article deals with the synthesis of mesoporous ordered material MCM-41 from sodium silicate. The series of MCM-41 materials are prepared from industrial sodium silicate using cetyltrimethylammonium bromide (CTAB) as a template and characterized by $N_2$ physisorption and small-angle X-Ray scattering. The MCM-41 sample prepared from the sodium silicate is characterized by high values of specific surface area (1118–1513 $m^2/g$), pore volumes (0.81–0.96 $cm^3/g$), and a well-ordered structure. It was found that the primary assembly of the ordered MCM-41 structure occurs in the solution at room temperature and the MCM-41 may be prepared from the sodium silicate even without hydrothermal treatment. The MCM-41 with a well-ordered structure and a narrow pore size distribution may be synthesized even at a very low CTAB/Si ratio of 0.025–0.125. The MCM-41 prepared from the sodium silicate is stable up to 700 °C and the specific surface area and pore volume were decreased only after the calcination at 800 °C. Thus, the MCM-41 synthesized from the sodium silicate at low CTAB/Si ratio is a promising cheap material for sorption, catalysis and other applications.

## Graphical Abstract

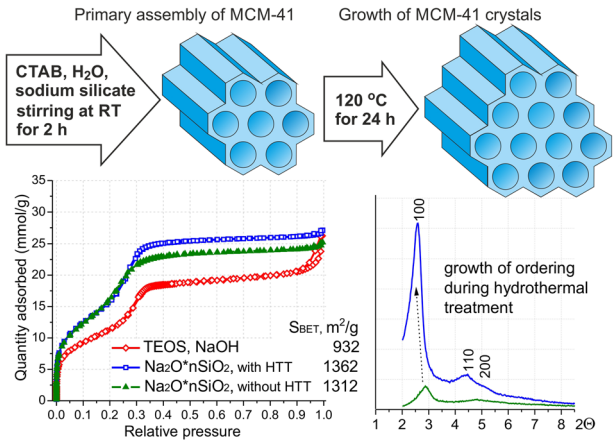


✉ G. V. Mamontov
GrigoriyMamontov@mail.ru

[1] Tomsk State University, Lenin Avenue, 36, Tomsk 634050, Russia

[2] Boreskov Institute of Catalysis, Siberian Branch of Russian Academy of Sciences, Prospekt Akademika Lavrentieva 5, Novosibirsk 630090, Russia

[3] Novosibirsk State University, Pirogova Street 2, Novosibirsk 630090, Russia

**Highlights**

- The MCM-41 material with well-ordered structure was prepared from sodium silicate.
- Decreasing of CTAB/Si ratio from 0.4 to 0.05 leads to narrower pore size distribution.
- The MCM-41 prepared from sodium silicate is stable up to 700 °C.

**Keywords** MCM-41 · Sodium silicate · CTAB/Si ratio · Well-ordered structure · Mesoporous silica

## 1 Introduction

The MCM-41 is a mesoporous ordered silica material from the MS41 family developed by the Mobil Oil Corporation in 1992 [1]. The MCM-41 material has a hexagonal-ordered structure with mesopores with sizes of 3–5 nm. The MCM-41 is a promising material for application because of its high specific surface area (above 1000 $m^2$/g) and a pore volume of ~1 $cm^3$/g. The MCM-41 is successfully used for sorption of organic pollutants from air due to relatively large pores that provide an easy mass transfer [2]. The mass uptake of the volatile organic compounds (VOCs) for MCM-41 was shown to exceed those for SBA-15 and other commercial sorbents based on silica, carbon, and polymers [3, 4]. The structure and functional properties of the MCM-41 can be changed significantly by a direct or post modification [5]. More often, the active organic functional groups are immobilized by grafting on the inner surface of the material [6]. The high surface area and large pores of the MCM-41 allow creating organically functionalized mesoporous silica with the high concentration of the active groups per mass of the material [7]. Such materials may be used for sorption of heavy metals [8, 9] and other water pollutants [10]. The opportunity to create the biocompatible MCM-41-based materials increases the interest to MCM-41 for drug delivery applications [11]. The slow rate of drug release from the porous structure of MCM-41 is used in their delivery to cancer cells [12, 13]. Due to small sizes of the active component nanoparticles formed inside the narrow MCM-41 pores [14, 15], the MCM-41-supported metals and metal oxides are promising catalysts in organic synthesis [16, 17], catalytic purification of air from VOCs [18], green energy [19], etc.

The synthesis of the MCM-41 involves few processes and the structure of resulting material significantly depends on the conditions: silica precursor, CTAB/Si ratio [20], hydrothermal treatment (HTT) [21], etc. Surfactants are often removed by calcination, or burning, to produce molecular sieves with narrow pore size distributions and highly ordered mesostructures. When extraction of templates is used instead of calcinations, organic functional groups can be incorporated into the materials during synthesis. The MCM-41 is synthesized by the templating method based on the formation of the inorganic–organic composites from the surfactant molecules and silicate framework. The cetyltrimethylammonium bromide (CTAB) is used as a template [1] and silicate highly ordered mesoporous system is assembled on the micelles of the CTAB. The calcination removes organic component and silica maintains the hard-ordered mesoporous structure. The synthesis can utilize different silica precursors: tetraethyl ortosilicate (TEOS), metasilicate, fumed silica, etc. The synthesis of MCM-41 from TEOS has been described in literature in details [3] and occurs under basic conditions and sodium or ammonia hydroxides can be used as a basic catalyst. $Na^+$ cations are assumed to create the ordered structure of MCM-41 silica [22]. The MCM-41 synthesis from TEOS is limited because of expensive TEOS and high amount of the required CTAB. The alkyl-silicate precursors also pollute the environment, which limits their application in a large-scale manufacturing [23].

Some publications are devoted to the use of alternative precursors, including sodium silicates [24, 25]. The idea to recycle the silica wastes, fly ash, rice husk, and diatomite through the preparation of MCM-41 may have important economical and environmental implications [26]. The presence of aluminum and other impurities (Mg, Ca, Fe, etc.) makes MCM-41 silica more active and stable [27, 28]. The influence of the sodium impurities on the MCM-41 properties is also very important, and it was found that the loading of sodium above 0.1 wt% makes MCM-41 material more unstable to water vapor [29]. Thus, the sodium silicate is an eco-friendly and cheap alternative precursor of silica, but the influence of conditions of synthesis and the loading of sodium should be taken into account. The change of the precursor from TEOS to sodium silicate requires the optimization of conditions of the synthesis: the amount of solvent, the CTAB/Si ratio, and the hydrothermal treatment that determines the structure of the resulting MCM-41. The additional way to reduce the cost of MCM-41 is to reduce the CTAB concentration, but the systematic studies are required.

The present work is devoted to the synthesis of the MCM-41 material from sodium silicate as a cheap and eco-friendly precursor of silica. In this paper, we reduce the CTAB/Si ratio from generally used 0.4 to up to 0.025. The study is related to the cheapening of MCM-41 production and the searching for optimal conditions to synthesize the MCM-41 from sodium silicate.

## 2 Materials and methods

In the present work, MCM-41 was prepared using an industrial sodium silicate with a module Si/Na = 1.5 (Salavat Catalyst Plant) and TEOS (chemically pure) as a silica precursors. The CTAB (minimum 99%, Sigma-Aldrich) was used as a template. The first series of MCM-41 was synthesized using TEOS and sodium silicate as silica precursors. The molar ratio of components was used to minimize the amount of CTAB [30] and it was the same for synthesis from TEOS and sodium silicate: 525($H_2O$):0.125 (CTAB):1(Si). The ammonia hydroxide (chemically pure) or sodium hydroxide (chemically pure) were dissolved in 850 ml of distilled water to obtain the pH ≈ 11, then the CTAB (4.09 g) was added and the mixture was stirred during 1 h for total dissolution of the CTAB. Then TEOS (18.73 g) was added and the mixture was stirred during 2 h at room temperature and then placed into an autoclave and exposed at 110 °C for 16 h. The solid product was filtered, washed with distilled water, dried at ambient temperature and calcined in air at a heating rate of 1 °C/min, and exposed at 540 °C for 10 h. The synthesis from the sodium silicate was carried out without the catalysts, since the pH of the aqueous solution of CTAB and sodium silicate was about 11. All conditions of the MCM-41 synthesis from sodium silicate were similar to those for the sample prepared from TEOS.

The second series of samples were synthesized from sodium silicate using molar ratio of components: 4200X ($H_2O$):X(CTAB):1(Si), where X was 0.025; 0.05; 0.075; 0.1; 0.125; 0.2; and 0.4. All conditions were similar to those used in the first series. To study the thermal stability of the MCM-41, the sample with a CTAB/Si ratio of 0.075 was calcined at 540, 600, 700, or 800 °C for 10 h.

The structure of the samples was studied by nitrogen sorption, powder XRD, and small-angle X-ray scattering (SAXS). Nitrogen adsorption–desorption isotherms of the MCM-41 samples were measured by "3Flex" analyzer from $p/p^\circ = 10^{-6}$ by fine adjustment of the $N_2$ portions and precision detecting of the pressure. The samples were outgassed at 200 °C for 2 h prior to the analysis. The specific surface area was calculated by straightening of the adsorption isotherm in Brunauer–Emmett–Teller (BET) coordinates in the range from 0.05 to 0.20 [31]. The pore size distributions for the MCM-41 were calculated by BJH-Desorption method (mesopores) or by density functional theory combined with non-negative regularization (DFT method) with $N_2$-Cylindrical Pores-Oxide Surface model [32].

XRD studies were carried out using Miniflex 600 diffractometer (Riguku) applying CuKα radiation ($\lambda$ = 1.5418 Å) with a monochromator, a scanning rate of 0.2 deg/min in the range of 2θ from 2° to 90°. SAXS patterns were registered by a S3-MICRO diffractometer (Hecus, Austria) with a Cu anode ($\lambda_{CuK\alpha}$ = 1.541 Å) and the point collimation system. The scattering vector magnitude $q = 4\pi \sin(\theta)/\lambda$ (where 2θ is the scattering angle, and $\lambda$ = 1.541 Å is the radiation wavelength) was used as the scattering coordinate. The scattering intensity was measured in the range of the scattering vector magnitudes $0.01 < q < 0.6$ Å$^{-1}$. The powder samples were placed in special cuvette with scatterless thin polymeric walls. The cell parameter $a$ (nm) was evaluated from the (100) reflection [1]. The pore wall thickness value $b$, was calculated by subtracting pore diameter value (nm) from the cell parameter $a$ (nm) by using the equation from reference [24]. The chemical composition of sample was studied by X-ray fluorescence analysis using the XRF-1800 spectrometer (Shimadzu, Japan).

## 3 Results and discussion

### 3.1 Synthesis of MCM-41 from TEOS and sodium silicate

The ratio of CTAB/Si = 0.2–0.7 is usually used to synthesize MCM-41. To minimize the amount of CTAB, the synthesis of MCM-41 from TEOS with a low amount of CTAB was carried out by Cai et al. [30] using the molar ratio CTAB/Si = 0.125. To explore the opportunity to prepare MCM-41 from sodium silicate using the same low CTAB/Si ratio of 0.125, the synthesis of MCM-41 from both TEOS (NaOH or $NH_4OH$ as a catalyst) and sodium silicate (without an alkali catalyst) was carried out. Figure 1 shows the isotherms of nitrogen adsorption–desorption for the synthesized samples.

The isotherms are characterized by an intensive growth of sorption at relative pressure below 0.02 that is attributed to high surface area of the samples (Table 1). The samples prepared from TEOS are characterized by $S_{BET}$ of 824 and 932 m$^2$/g, while those made from sodium silicate have $S_{BET}$ of 1312 and 1362 m$^2$/g. The step on the isotherms at relative pressures from 0.2 to 0.4 is attributed to the presence of narrow mesopores that is typical for the MCM-41 material [33]. A hysteresis loop at relative pressures of 0.85–1.0 for the samples prepared from TEOS indicates the presence of wide mesopores. The nitrogen adsorption–desorption isotherm for the sample prepared from sodium silicate is fully reversible that indicates the presence of the material with the ordered pore system without the additional wide mesopores. It can be seen from the pore size distributions (Fig. 1b) that narrow pores from 2.5 to 4.3 nm are predominant in the structure of the samples that confirms the formation of the material with the MCM-41 structure. Besides, the additional amount of mesopores with sizes of 10–60 nm is observed for the samples prepared from TEOS.

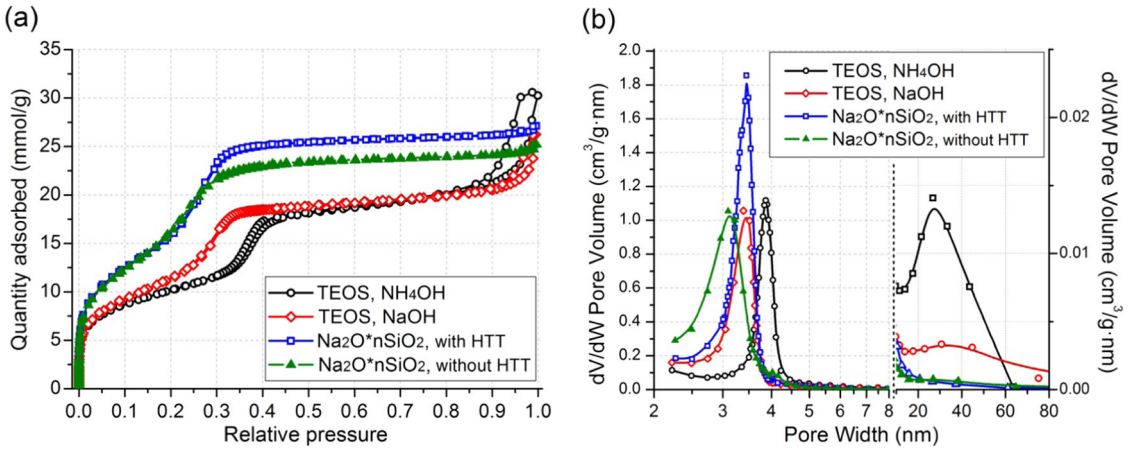


**Fig. 1** The nitrogen adsorption–desorption isotherms (**a**) and the corresponding pore size distributions (BJH-Desorption method) (**b**) for MCM-41 samples synthesized from TEOS and sodium silicate

**Table 1** The textural characteristics of MCM-41 synthesized from TEOS and sodium silicate

| Samples | $S_{BET}$ ($m^2$/g) | $V_{pore}$ ($cm^3$/g) | $D_{pore}$ (nm)[a] | $D_{pore>5\,nm}$ (nm)[b] | $W_{1/2\,h}$ (nm) |
|---|---|---|---|---|---|
| TEOS_$NH_4OH$ | 824 | 0.99 | 3.87 | 26.89 | 0.46 |
| TEOS_NaOH | 932 | 0.84 | 3.45 | 37.05 | 0.50 |
| $Na_2O$ $nSiO_2$ (with HTT) | 1362 | 0.93 | 3.26 | – | 0.42 |
| $Na_2O$ $nSiO_2$ (without HTT) | 1312 | 0.86 | 3.14 | – | 0.74 |

[a]Maximum of pore size distribution according to BJH-Desorption method

[b]Second maximum of pore size distribution according to BJH-Desorption method

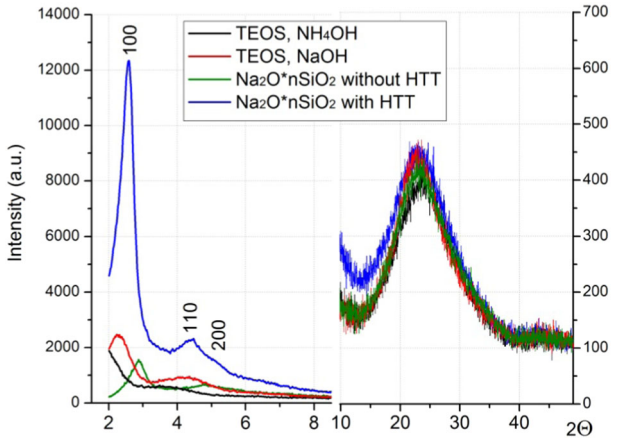


**Fig. 2** The XRD patterns of MCM-41 samples prepared from TEOS and sodium silicate

The use of the $NH_4OH$ as catalysts leads to the formation of MCM-41 with narrower pore size distribution; however, the amount of wide mesopores is also higher for this sample.

Figure 2 shows the XRD patterns from 2θ of 2°. The wide halo at 10–35° is the same for all samples and can be attributed to the amorphous structure of the silica. The reflections at angles from 2 to 8° correspond to the hexagonal MCM-41 structure [31]. It can be seen from the XRD patterns that the intensity of the reflections in a small-angle range is significantly higher for the MCM-41 prepared from the sodium silicate. This indicates a higher order of the structure of MCM-41 synthesized from sodium silicate in comparison with the one synthesized from TEOS under the same conditions.

Two main mechanisms of assembly of the MCM-41 structure in the solution are known [1]. The first mechanism includes the formation of liquid crystals of hexagonal packed cylindrical micelles of CTAB followed by condensation of silicate species onto the external surface [34]. The second mechanism is based on the formation of the cylindrical micelles of CTAB and their spontaneous packing/assembly into a highly ordered mesoporous phase with an energetically favorable hexagonal arrangement accompanied by the silicate condensation [34, 35].

To study the possible route of the MCM-41 assembly from the sodium silicate at a relatively low CTAB/Si ratio, the synthesis of the materials without HTT was carried out. The mixture of sodium silicate with CTAB with a molar ratio of 525($H_2O$):0.125(CTAB):1(Si) was stirred during 2 h at room temperature and then filtered, washed, and calcined at 540 °C. It can be seen from the $N_2$ adsorption–desorption isotherm (Fig. 1a) that the sample ***$Na_2O$ $nSiO_2$ without HTT*** has the same shape of isotherm that indicates the assembly of the ordered structure from the

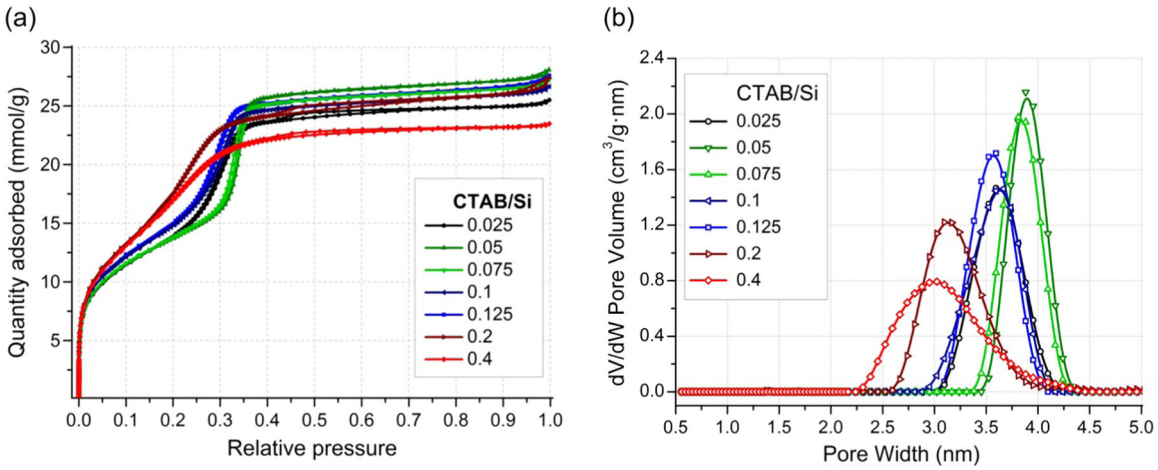


**Fig. 3** The isotherms of $N_2$ adsorption–desorption (**a**) and pore size distributions (**b**) for MCM-41 synthesized with different CTAB/Si ratio

sodium silicate in the solution even without hydrothermal conditions. This sample has insignificantly smaller $S_{BET}$ and pore volume values (Table 1), and the pore size distribution is shifted towards smaller sizes (a maximum of pore size distribution at 3.14 nm). Figure 2 shows the XRD pattern for this sample. The reflections of the hexagonal MCM-41 structure appear, while their intensity is smaller in comparison with the one for the same sample prepared with a HTT. Therefore, the formation of the ordered well-organized cylinders occurs in the solution, and the HTT provides the subsequent growth of the MCM-41 particles with the corresponding ordering enhancement.

Thus, it can be concluded from the obtained results that silica with structure of MCM-41 may be prepared from sodium silicate using low amount of CTAB (CTAB/Si = 0.125) even without HTT. The prepared MCM-41 is characterized by higher $S_{BET}$, narrow pore size distribution, and a well-ordered structure. The easy formation of the well-ordered material MCM-41 from sodium silicate may be associated with a self-assembly of the hexagonal structure from the CTAB and silicate species under these conditions. The assembly of TEOS-derived MCM-41 structure is limited by two reactions: a hydrolysis of TEOS and a condensation of silicate monomers. Probably, the molar ratio of CTAB/Si = 0.125 is low to form only MCM-41 from TEOS, and a competitive formation of the unordered large silica particles occurs under basic conditions. The assembly of the ordered structure of the MCM-41 made from sodium silicate is easy due to the presence of the predominantly monomeric silicate species in this solution at pH ≈ 11.

### 3.2 Synthesis of MCM-41 from sodium silicate using different CTAB/Si ratio

To study the influence of the CTAB/Si molar ratio on the structure of MCM-41, the series of samples were synthesized from sodium silicate using CTAB/Si ratio from 0.025 to 0.4. The CTAB/$H_2O$ ratio was of 1/4200 for all samples in these series to keep the same state of the CTAB micelles in the solution as in the first series of samples. Figure 3a shows the isotherms of nitrogen adsorption–desorption and pore size distributions for the synthesized series of samples. All isotherms may be assigned to type IV isotherms with type H1 hysteresis loop according to IUPAC recommendations [36, 37]. The high nitrogen uptake at a relative pressure of 0.2–0.35 is attributed to capillary condensation in narrow cylindrical mesopores that is typical for the MCM-41 material [31]. Thus, the observed shape of the isotherms confirms the preparation of the samples with the structure of MCM-41. The isotherms for the samples obtained with the CTAB/Si ratio of 0.2 and 0.4 are characterized by a relatively shallow slope of the isotherms at 0.15–0.3, while the one for the samples with CTAB/Si = 0.025–0.125 is sharper and shifted to 0.25–0.35. This indicated the formation of the structure with more uniform and large mesopores.

Figure 3b shows the pore size distributions (DFT method) for the synthesized samples. Narrow pore size distributions from 2.3 to 4.3 nm are observed for all samples that indicate the formation of the materials with the uniform pores. The wider pore size distribution from 2.3 to 4.3 nm with a maximum at ~3 nm is observed for the sample prepared with a CTAB/Si molar ratio of 0.4. The decreasing of the CTAB/Si leads to narrower pore size distributions and a shift of maximum of distribution at higher width to up to ~3.9 nm for the sample with the CTAB/Si ratio of 0.05. The peak width at the ½ height ($\mathbf{W_{1/2}}$) is 0.42 nm for this sample (Table 2). The regular decreasing of $W_{1/2}$ from 0.94 to 0.42 nm with a decreasing of the CTAB/Si ratio from 0.4 to 0.05 takes place, and a more homogeneous porous structure is formed in case of the sample with the CTAB/Si ratio of 0.05.

**Table 2** The textural characteristics of MCM-41 with different CTAB/Si ratio

| CTAB/ Si ratio | $S_{BET}$ ($m^2$/g) | $V_{pore}$ ($cm^3$/g) | $D_{pore}$ (nm)[a] | $W_{1/2\,h}$ (nm) | Cell parameter *a* (nm) | Wall thickness (nm) |
|---|---|---|---|---|---|---|
| 0.025 | 1136 | 0.88 | 3.62 | 0.57 | 4.22 | 0.91 |
| 0.05 | 1118 | 0.96 | 3.87 | 0.42 | 4.62 | 0.94 |
| 0.075 | 1126 | 0.93 | 3.83 | 0.46 | 4.48 | 0.93 |
| 0.1 | 1222 | 0.91 | 3.62 | 0.59 | 4.32 | 0.91 |
| 0.125 | 1229 | 0.94 | 3.58 | 0.51 | 4.17 | 0.86 |
| 0.2 | 1513 | 0.92 | 3.14 | 0.65 | 3.70 | 0.78 |
| 0.4 | 1456 | 0.81 | 3.02 | 0.94 | 3.57 | 0.82 |

[a]Maximum of pore size distribution according to DFT method

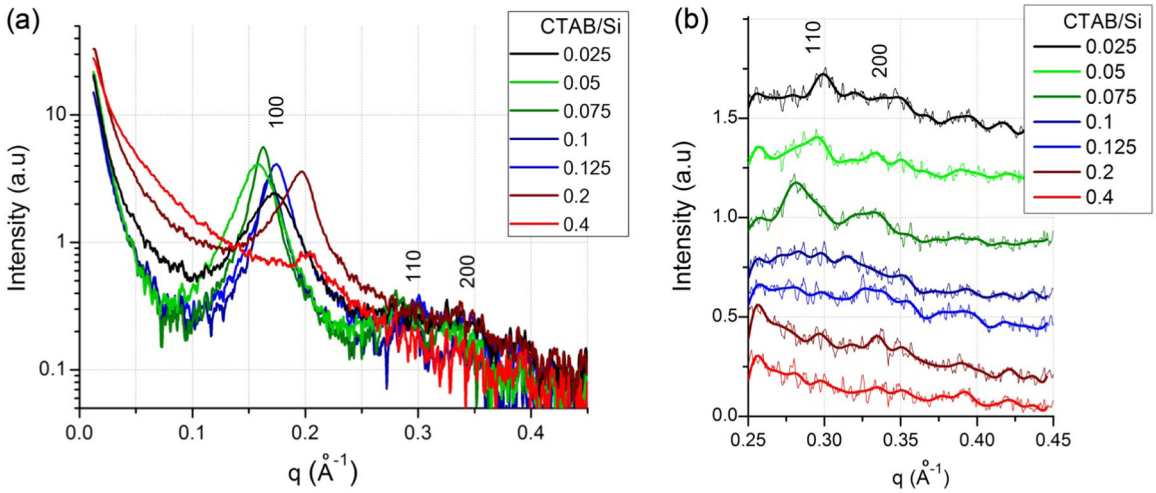


**Fig. 4** SAXS patterns of MCM-41 synthesized with different CTAB/Si ratio

The decreasing of the CTAB/Si ratio up to 0.025 leads to a reverse shift of the pore size distribution to 3.0–4.1 nm with the increase of the $W_{1/2}$ value up to 0.57 nm. Thus, introduction of an extremely small amount of CTAB (CTAB/Si < 0.05) leads to decreasing of the homogeneity in the structure of MCM-41 material prepared from sodium silicate. Probably, this is attributed to the assembly and polymerization of silica precursor both over CTAB micelles and without CTAB. The thin hysteresis loop from 0.45 to 0.6 is observed on the isotherm for sample with the CTAB/Si ratio of 0.025 (Fig. 3a). This hysteresis loop indicates the formation of thin mesopores with geometry that differs from cylindrical pores of MCM-41. Thus, the porous structure of the sample with the CTAB/Si ratio of 0.025 is less homogeneous due to presence of two types of thin mesopores.

Figure 4 shows the SAXS patterns for the synthesized series of MCM-41 samples. The presence of peaks for all samples confirms the formation of the ordered hexagonal MCM-41 structure [1, 20]. The cell parameter *a* calculated from SAXS data is in the range from 3.57 to 4.62 nm (Table 2). The sample prepared with the CTAB/Si ratio of 0.4 is characterized by a low intensity of $d_{100}$ peak that indicates the low-ordered structure in comparison with other samples. The cell parameter for this sample is the smallest one (3.57 nm) that is in agreement with the sorption results. The decreasing of the CTAB/Si ratio leads to rise of intensity of this peak and its shift to smaller angles. The corresponding increasing of the cell parameter is observed with a maximal value for the sample with the CTAB/Si = 0.05 ($a = 4.62$ nm). The high intensity and narrowness of this peak for the samples with the CTAB/Si ratio <0.4 indicate a well-ordered MCM-41 structure. However, the CTAB/Si = 0.025 sample is characterized by the peak shifted to larger angles, the cell parameter decreases to up to 4.22 nm. Generally, SAXS results are in good agreement with the results of $N_2$ adsorption and confirms the well-ordered structure for the samples with the CTAB/Si ratio <0.4.

The textural characteristics of these series MCM-41 are summarized in Table 2 and dependencies of characteristics from CTAB/Si ratio are shown in Fig. 5. All samples have high specific surface areas (1118–1513 $m^2$/g) and pore volumes (0.81–0.96 $cm^3$/g). It was found that increasing of CTAB/Si ratio from 0.05 to 0.2 led to rising of the specific surface area (the value of error of the method is less than 5 relative percents, the error bars are shown in Fig.5). This is

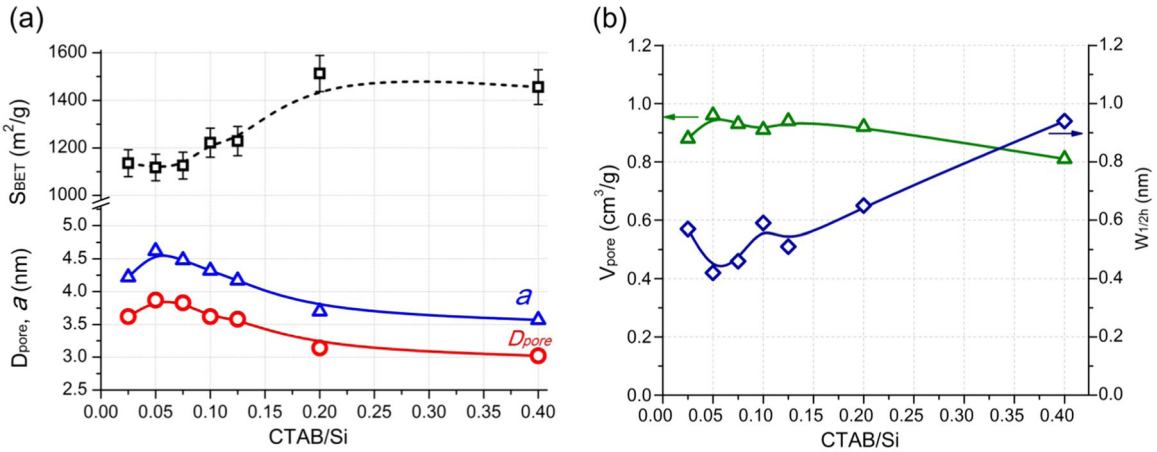


**Fig. 5** The dependences of the textural characteristics of MCM-41 on the CTAB/Si ratio

accompanied with decreasing of cell parameter and average pore size (Fig. 5a). Thus, the $S_{BET}$ is a function of the pore diameter for the synthesized series of MCM-41. The pore diameter ($D_{pore}$) is changed insignificantly (Fig. 5b), but the maximal $V_{pore} = 0.96\ cm^3/g$ is observed for the sample with the CTAB/Si = 0.05, and a minimal $V_{pore} = 0.81\ cm^3/g$ is observed for the sample with the CTAB/Si = 0.4. Regardless of the smallest specific surface area 1118 and 1126 $m^2/g$ for the samples with the CTAB/Si ratio of 0.05 and 0.075, respectively, these two samples are characterized by the narrowest pore size distribution and the minimal $W_{1/2h}$ value (0.42 and 0.46 nm, respectively). This indicates the most homogeneous ordered structure compared to other samples. Similar small $W_{1/2h}$ values for the MCM-41 were achieved by Lin in reference [21] during the synthesis of MCM-41 from sodium silicate with the CTAB/Si ratio of ~0.4 CTAB/Si and HTT for 10–30 days. Also, the growth of the wall thickness with a decreasing of the CTAB/Si ratio is observed (Table 2) that may be caused by the increased amount of silica which was formed on the surface of the CTAB micelles from the adsorbed silicate species. The formation of loose swelled silica occurs during HTT and the wall thickness of primary assembled MCM-41 is determined by amount of silicate species absorbed onto CTAB micelles. The calcination leads to both burning of CTAB and compaction of silica carcass. This leads to increasing of pore size and cell parameter *a*.

Thus, both increased pore size and wall thickness for samples prepared with low CTAB/Si ratio are a result of high amount of silicate species assembled onto CTAB micelles. It was shown above that the primary assembly of MCM-41 occurs in the solution. The $H_2O$/CTAB ratio of 1/4200 was kept in this series of samples, and the formation of similar CTAB micelles in solution and similar diameter of primary channels in the CTAB@MCM-41 hybrid composite are expected. The thickness of the primary silica–gel walls depends on the amount of silica precursors and is higher for the samples with small CTAB/Si ratio. The heating of the sample during the calcination leads to a significant compacting of the silica wall due to polycondensation processes, release of water, and increasing of density. Therefore, the decreasing of the wall thickness and corresponding growth of pore diameter are expected during the calcination. Thus, the maximal compaction of the silica–gel wall is observed for sample with the highest amount of silica and the corresponding largest wall thickness, i.e., the samples with small CTAB/Si ratio (0.05 and 0.075). This explains the widest pore diameter for these samples.

Thus, the CTAB/Si ratio affects the textural characteristics of the MCM-41 prepared from the sodium silicate. The CTAB/Si ratio of 0.2–0.4 provides the synthesis of MCM-41 with higher specific surface area (1456–1513 $m^2/g$) and smaller pore sizes (maximum of pore size distribution at 3.02–3.14 nm). The homogeneity of the structure of these samples is not high, and a small intensity of the SAXS peak and a relatively wide pore size distribution are observed. The decreasing of the CTAB/Si ratio to up to 0.05–0.125 provides the decreasing of the $S_{BET}$ to up to 1118–1229 $m^2/g$, increasing of the pore diameter to up to 3.58–3.87 nm, but the high homogeneity of the porous structure is observed. Thus, the MCM-41 with a well-ordered porous structure may be synthesized even at a very low CTAB/Si ratio.

### 3.3 Effect of calcination temperature on the MCM-41 structure

It is known that the main disadvantage of the MCM-41 synthesized from sodium silicate is the presence of $Na^+$ impurities which leads to a low thermal stability [29]. The chemical composition of the sample synthesized with the

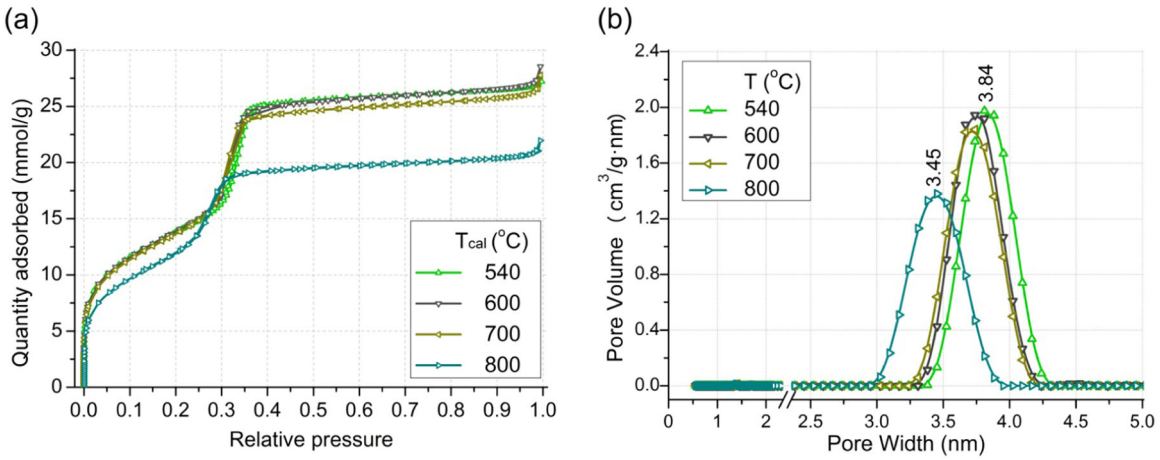


**Fig. 6** The isotherms of $N_2$ adsorption-desorption (**a**) and pore size distributions (**b**) for MCM-41 exposed to different temperatures

**Table 3** The textural characteristics of MCM-41 after calcination at different temperatures

| $T_{cal}$ (°C) | $S_{BET}$ ($m^2$/g) | $D_{pore}$ (nm)[a] | a (nm) | Wall thickness (nm) | $V_{pore}$ ($cm^3$/g) | $W_{1/2\,h}$ (nm) |
|---|---|---|---|---|---|---|
| 540 | 1126 | 3.84 | 4.48 | 0.93 | 0.94 | 0.46 |
| 600 | 1131 | 3.75 | 4.42 | 0.91 | 0.94 | 0.42 |
| 700 | 1118 | 3.73 | 4.37 | 0.92 | 0.91 | 0.45 |
| 800 | 981 | 3.45 | 4.22 | 1.06 | 0.72 | 0.48 |

[a]Maximum of pore size distribution according to DFT method

CTAB/Si ratio of 0.075 was analyzed by XRF method. The loading of $Na^+$ is 0.04 wt% and can be attributed to a weak binding with the silica matrix and easy leaching during the washing.

The thermal stability of the MCM-41 was studied by comparing this sample after the calcination at 540, 600, 700, and 800 °C during 10 h. The isotherms of $N_2$ adsorption–desorption and the corresponding pore size distributions for MCM-41 are demonstrated in Fig. 6. The isotherms and textural characteristics ($S_{BET}$ and $V_{pore}$, see Table 3) for samples calcined at 540, 600, and 700 °C are similar. This indicates the good stability of the MCM-41 synthesized from sodium silicate at temperatures up to 700 °C. The isotherm for MCM-41 after the calcination at 800 °C is characterized by both a decreased adsorption value and a shift of the step from the relative pressures of 0.25–0.35 to 0.20–0.30. Figure 6b shows the shift of the pore size distribution to smaller width. The surface area for this sample decreased from 1118 to 981 $m^2$/g (Table 3) and the pore volume decreases from 0.94 to 0.71 $cm^3$/g. A dramatic decrease of the $S_{BET}$ from 1114 to up to 403 $m^2$/g with an increase of the calcination temperature from 650 to 750 °C was observed for the MCM-41 synthesized from TEOS [38]. When the fumed silica was used as a precursor, the decreasing of the $S_{BET}$ from 970 to up to 879 $m^2$/g was observed. Thus, the nature of the silica precursor influences on the thermal stability of the MCM-41.

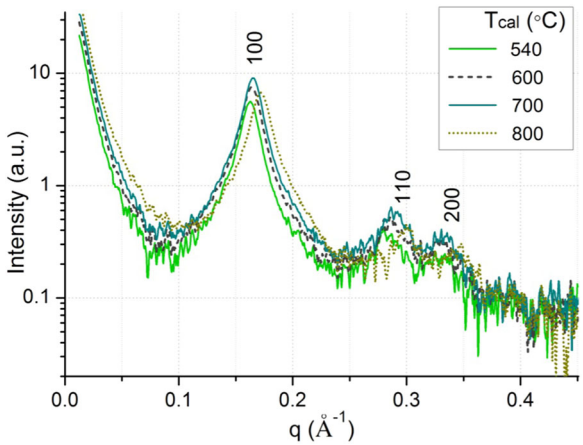


**Fig. 7** SAXS patterns of MCM-41 after calcination at different temperatures

Figure 7 demonstrates the SAXS patterns of the MCM-41 after calcination at different temperatures. There are no significant changes in the spectra that indicate the stability of the ordered structure. The insignificant shift of the reflections takes place for the MCM-41 after exposing at 800 °C. The cell parameter a decreases from 4.48 nm to 4.22 nm with a growth of the calcination temperature from 540 to 800 °C (Table 3). The wall thickness is stable after the calcination at 540, 600, and 700 °C (Table 3), while the increased wall thickness up to 1.06 nm is observed for the sample after the calcination at 800 °C. The decreased cell parameter and the pore diameter together with an increased value of wall thickness indicate the compression of the MCM-41 structure.

Thus, according to the $N_2$ sorption and SAXS data, the growth of the calcination temperature of the MCM-41

prepared from the sodium silicate to up to 700 °C does not lead to significant changes of its structure that indicates the high thermal stability. Only the calcination at 800 °C leads to the decreased $S_{BET}$ and $V_{pore}$ with a decreasing of the pore width due to the compression of the structure and partial degradation of the porous structure. On the other hand, the stability of the SAXS peaks intensity after the high-temperature treatment indicates the keeping of the ordered hexagonal structure. Therefore, the decreasing of the pore volume of pores with sizes of 3–4 nm (Fig. 6b) and $S_{BET}$ may be attributed to the blocking of the ends of the cylindrical pores. Thus, despite the small Na impurities, the high thermal stability of the MCM-41 allows using the prepared material in different high-temperature applications, including sorption and catalysis.

## 4 Conclusions

Thus, it was shown that the MCM-41 with a well-ordered structure and higher specific surface area can be synthesized from the sodium silicate even without the HTT. The MCM-41 synthesized from TEOS under the same conditions had lower surface area and a poor ordered structure. The influence of the CTAB/Si molar ratio from 0.025 to 0.4 on the MCM-41 structure was studied. It was found that the samples with a CTAB/Si ratio of 0.05–0.125 were characterized by the more homogeneous (narrow pore size distribution) and a well-ordered structure. The correlations between the CTAB/Si ratio and the $S_{BET}$, pore diameter, wall thickness, and cell parameter were revealed. It was established that the structure of the MCM-41 prepared from the sodium silicate was stable up to 700 °C, and the insignificant reduction of the textural characteristics was observed after the calcination at 800 °C.

To sum up, the synthesis of the MCM-41 from sodium silicate as an eco-friendly, cheap, and incombustible precursor and with the extremely low CTAB concentration provides the formation of the MCM-41 with a well-ordered structure, high textural characteristics, the narrow pore size distribution, and the high thermal stability. The elaborated approaches make the mesoporous ordered silica with the MCM-41 structure a promising material for a wide field of applications.

**Acknowledgements** This study was supported by "The Tomsk State University Academic D. I. Mendeleev Fund Program (grant No. 8.2.03.2018).

### Compliance with ethical standards

**Conflict of interest** The authors declare that they have no conflict of interest.



## References

1. Beck JS, Vartuli JC, Roth WJ, Leonowicz ME, Kresge CT, Schmitt KD, Chu CT-W, Olson DH, Sheppard EW, McCullen SB, Higgins JB, Schlenker JL (1992) A new family of mesoporous molecular sieves prepared with liquid crystal templates. J Am Chem Soc 114 (27):10834–10843. https://doi.org/10.1021/ja00053a020
2. Davis ME (2002) Ordered porous materials for emerging applications. Nature 417(6891):813–821. https://doi.org/10.1038/nature00785
3. Gibson LT (2014) Mesosilica materials and organic pollutant adsorption: part A removal from air. Chem Soc Rev 43 (15):5163–5172. https://doi.org/10.1039/c3cs60096c
4. Idris SA, Robertson C, Morris MA, Gibson LT (2010) A comparative study of selected sorbents for sampling of aromatic VOCs from indoor air. Anal Methods 2(11):1803–1809. https://doi.org/10.1039/c0ay00418a
5. Taguchi A, Schüth F (2005) Ordered mesoporous materials in catalysis. Microporous Mesoporous Mater 77(1):1–45. https://doi.org/10.1016/j.micromeso.2004.06.030
6. Albela B, Bonneviot L (2016) Surface molecular engineering in the confined space of template porous silica. New J Chem 40 (5):4115–4131. https://doi.org/10.1039/C5NJ03437J
7. Hoffmann F, Cornelius M, Morell J, Fröba M (2006) Silica-based mesoporous organic–inorganic hybrid materials. Angew Chem Int Ed 45(20): 3216–3251. https://doi.org/10.1002/anie.200503075
8. Da'na E (2017) Adsorption of heavy metals on functionalized-mesoporous silica: a review. Microporous and Mesoporous Mater 247:145–157. https://doi.org/10.1016/j.micromeso.2017.03.050
9. Idris SA, Davidson CM, McManamon C, Morris MA, Anderson P, Gibson LT (2010) Large pore diameter MCM-41 and its application for lead removal from aqueous media. J Hazard Mater 185(2–3):898–904. https://doi.org/10.1016/j.jhazmat.2010.09.105
10. Gibson LT (2014) Mesosilica materials and organic pollutant adsorption: part B removal from aqueous solution. Chem Soc Rev 43(15):5173–5182. https://doi.org/10.1039/c3cs60095e
11. Slowing II, Vivero-Escoto JL, Wu C-W, Lin VS-Y (2008) Mesoporous silica nanoparticles as controlled release drug delivery and gene transfection carriers. Adv Drug Deliv Rev 60 (11):1278–1288. https://doi.org/10.1016/j.addr.2008.03.012
12. Freitas LB de O, Bravo IJG, Macedo WA de A, de Sousa EMB (2015) Mesoporous silica materials functionalized with folic acid: preparation, characterization and release profile study with methotrexate. J Sol-Gel Sci Technol 43(15):5173–5182. https://doi.org/10.1007/s10971-015-3844-8
13. Latifi L, Sohrabnezhad S (2018) Influence of pore size and surface area of mesoporous silica materilas (MCM-41 and KIT-6) on the drug loading and release. J Sol-Gel Sci Technol 87(3):626–638. https://doi.org/10.1007/s10971-018-4742-7
14. Abu Bakar NHH, Bettahar MM, Abu Bakar M, Monteverdi S, Ismail J (2010) Low temperature activation of Pt/Ni supported MCM-41 catalysts for hydrogenation of benzene. J Mol Catal A Chem 333 (1–2):11–19. https://doi.org/10.1016/j.molcata.2010.10.007
15. Mamontov GV, Gorbunova AS, Vyshegorodtseva EV, Zaikovskii VI, Vodyankina OV Selective oxidation of CO in the presence of propylene over Ag/MCM-41 catalyst Catal Today (in press). https://doi.org/10.1016/j.cattod.2018.05.015
16. Silvestre-Albero J, Serrano-Ruiz JC, Sepúlveda-Escribano A, Rodríguez-Reinoso F (2008) Zn-modified MCM-41 as support for Pt catalysts. Appl Catal A 351(1):16–23. https://doi.org/10.1016/j.apcata.2008.08.021

17. You, S, Huang, B, Yan, T, Cai, M (2018) A highly efficient heterogeneous palladium-catalyzed carbonylative annulation of 2-aminobenzamides with aryl iodides leading to quinazolinones. J Organomet Chem 875:35–45. https://doi.org/10.1016/j.jorganchem.2018.09.003
18. Marin ML, Santos-Juanes L, Arques A, Amat AM, Miranda MA (2011) Organic photocatalysts for the oxidation of pollutants and model compounds. Chem Rev 112(3):1710–1750. https://doi.org/10.1021/cr2000543
19. Linares N, Silvestre-Albero AM, Serrano E, Silvestre-Albero J, García-Martínez J (2014) Mesoporous materials for clean energy technologies. Chem Soc Rev 43(22):7681–7717. https://doi.org/10.1039/c3cs60435g
20. Kresge CT, Roth WJ (2013) The discovery of mesoporous molecular sieves from the twenty year perspective. Chem Soc Rev 42(9):3663–3670. https://doi.org/10.1039/c3cs60016e
21. Lin HP, Cheng S, Mou C-Y (1996) Synthesis of thermally stable MCM-41 at ambient temperature. J Chin Chern Soc 43 (5):375–378. https://doi.org/10.1002/jccs.199600054
22. Kirik SD, Belousov OV, Parfenov VA, Vershinina MA (2005) System approach to analysis of the role of the synthesis components and stability of the MCM-41 mesostructured silicate material. Glass Phys and Chem 31(4):439–451. https://doi.org/10.1007/s10720-005-0081-1
23. Yang G, Deng Y, Ding H, Lin Z, Shao Y, Wang Y (2015) A facile approach to synthesize MCM-41mesoporous materials from iron ore tailing: influence of the synthesis conditions on the structural properties. Appl Clay Sci 111:61–66. https://doi.org/10.1016/j.clay.2015.04.005
24. Kruk M, Jaroniec M, Sakamoto Y, Terasaki O, Ryoo R, and Ko CH (2000) Determination of pore size and pore wall structure of MCM-41 by using nitrogen adsorption, transmission electron microscopy, and X-ray diffraction. J Phys Chem B 104 (2):292–301. https://doi.org/10.1021/jp992718a
25. Mokhonoana MP, Coville NJ (2010) Synthesis of [Si]-MCM-41 from TEOS and water glass: the water glass-enhanced condensation of TEOS under alkaline conditions. J Sol-Gel Sci Technol 54(1):83–92. https://doi.org/10.1007/s10971-010-2161-5
26. Halinaa M, Ramesh S, Yarmo MA, Kamarudin RA (2007) Non-hydrothermal synthesis of mesoporous materials using sodium silicate from coal fly ash. Mater Chem Phys 101(2–3):344–351. https://doi.org/10.1016/j.matchemphys.2006.06.007
27. Boger T, Roesky R, Gläser R, Ernst S, Eigenberger G, Weitkamp J (1997) Influence of the aluminum content on the adsorptive properties of MCM-41. Microporous Mater 8(1–2):79–91. https://doi.org/10.1016/S0927-6513(96)00061-2
28. Inagaki S, Fukushima Y, Kuroda K (1993) Synthesis of highly ordered mesoporous materials from a layered polysilicate. J Chem Soc Chem Commun (8):680–682. https://doi.org/10.1039/C39930000680
29. Pauly TR, Petkov V, Liu Y, Billinge SJL, Pinnavaia TJ (2004) Role of framework sodium versus local framework structure in determining the hydrothermal stability of MCM-41 mesostructures. J Am Chem Soc 124(1):97–103. https://doi.org/10.1021/ja0118183
30. Cai Q, Lin W-Y, Xiao F-S, Pang W-Q, Chen X-H, Zou B-S (1999) The preparation of highly ordered MCM-41 with extremely low surfactant concentration. Microporous Mesoporous Mater 32 (1–2):1–15. https://doi.org/10.1016/S1387-1811(99)00082-7
31. Meynen V, Cool P, Vansant EF (2009) Verified syntheses of mesoporous materials. Microporous Mesoporous Mater 125 (3):170–223. https://doi.org/10.1016/j.micromeso.2009.03.046
32. Landers J, Gor GY, Neimark AV (2013) Density functional theory methods for characterization of porous materials. 437:3–32. https://doi.org/10.1016/j.colsurfa.2013.01.007
33. Storck S, Bretinger HF, Maier WF (1998) Characterization of micro- and mesoporous solids by physisorption methods and pore-size analysis. Appl Catal A 174(1–2):137–146. https://doi.org/10.1016/S0926-860X(98)00164-1
34. ALOthman Z (2012) A review: fundamental aspects of silicate mesoporous materials. Materials 5(12):2874–2902. https://doi.org/10.3390/ma5122874
35. Chen C-Y, Burkett SL, Li H-X, Davis ME (1993) Studies on mesoporous materials II. Synthesis mechanism of MCM-41. Microporous Mater 2(1):27–34. https://doi.org/10.1016/0927-6513(93)80059-4
36. Sing KS, Everett DH, Haul RA, Moscou L, Pierotti RA, Rouquerol J, Siemicniewska T (1985) Reporting physisorption data for gas solidsystems with special reference to the determination of surface-area and porosity (Recommendations 1984). Pure Appl Chem 57:603–619. https://doi.org/10.1351/pac198557040603
37. Thommes M, Kaneko K, Neimark AV, Olivier JP, Rodriguez-Reinoso F, Rouquerol J, Sing KSW (2015) Physisorption of gases, with special reference to the evaluation of surface area and pore size distribution (IUPAC Technical Report). Pure Appl Chem 87 (9–10):1051–1069. https://doi.org/10.1515/pac-2014-1117
38. Cassiers K, Linssen T, Mathieu M, Benjelloun M, Schrijnemakers K, Van Der Voort P, Cool P, Vansant EF (2002) A detailed study of thermal, hydrothermal, and mechanical stabilities of a wide range of surfactant assembled mesoporous silicas. Chem Mater 14(5):2317–2324. https://doi.org/10.1021/cm0112892